INORGANIC CHEMISTRY FRONTIERS

RESEARCH ARTICLE

View Article Online
View Journal | View Issue

Cite this: *Inorg. Chem. Front.*, 2024, **11**, 6020

From $BaAlBO_3F_2$ to $BaAlB_3O_6F_2$ and $BaAl_2(B_3O_6)_2F_2$: the enhancement of birefringence and band gap by extending the π-conjugated system combined with [Al–O/F] functional groups†

Cheng Chen,[a] Danyang Dou,[a] Yunjie Bai,[a] Bingbing Zhang [a,b] and Ying Wang *[a,b]

Received 17th June 2024,
Accepted 28th July 2024

DOI: 10.1039/d4qi01530d

rsc.li/frontiers-inorganic

The investigation of birefringent materials is predominantly focused on π-conjugated systems; however, a large band gap or deep ultraviolet (DUV) transmittance cannot be guaranteed. In this work, we propose an extended π-conjugated strategy to increase the birefringence while keeping the large band gap. In the scheme, two new fluoroaluminoborates, $BaAlB_3O_6F_2$ and $BaAl_2(B_3O_6)_2F_2$, are synthesized by combining the $[BO_3]$ group with the $[AlO_4F_2]$ group and the $[B_3O_6]$ group with the $[AlO_3F]$ group through a rational structural design. The experimental results indicate that both $BaAlB_3O_6F_2$ and $BaAl_2(B_3O_6)_2F_2$ exhibit shorter UV cutoff wavelengths (<200 nm) and larger birefringence (Δn > 0.07@546 nm). Notably, this is a new finding in the Ba–Al–B–O–F system since the discovery of the well-known nonlinear optical crystal $BaAlBO_3F_2$. In comparison with $BaAlBO_3F_2$, $BaAlB_3O_6F_2$ and $BaAl_2(B_3O_6)_2F_2$ exhibit a markedly elevated birefringence (0.0418 *vs.* 0.087/0.105 at 546 nm). Furthermore, $BaAl_2(B_3O_6)_2F_2$ exhibits the largest band gap (7.87 eV) of all known F-containing aluminoborates. This work not only identifies two potential DUV birefringent materials, but also proposes a novel design approach for reconciling the conflicting properties between birefringence and bandgap.

Introduction

Birefringent crystals are of significant importance in the field of optical applications. They are key materials for the production of prisms, polarizers, lenses, precision optics, and electronic laser components.[1–6] Currently, some birefringent materials such as MgF_2,[7] $CaCO_3$,[8] α-BaB_2O_4,[9] YVO_4,[10] $LiNbO_3$,[11] and quartz crystals[10] are well developed and commercially available. However, the respective defects of these materials restrict their potential applications in the DUV (wavelengths less than 200 nm) range. For instance, MgF_2 and quartz crystals can be applied to DUV while their birefringence is relatively low. Conversely, $CaCO_3$, $LiNbO_3$ and YVO_4 exhibit high birefringence and are easily processed, but their operational wavelength is limited to the visible and near-infrared region. α-BaB_2O_4 possesses the requisite properties for DUV birefringent materials. However, its UV cut-off edge is only up to 189 nm, and crystal growth is challenging due to phase transition. Two essential prerequisites for the development of DUV birefringent materials are an adequate band gap and a sufficient birefringence.[12] However, it is a difficult problem to balance these two conflicting properties. Consequently, it remains imperative to identify DUV birefringent materials with optimized optical properties.

To search new DUV birefringent materials, the rational selection of functional groups in the structure of crystalline materials is a key factor.[13–16] For example, in the borate structure, the large electronegativity difference between B and O atoms gives it a wide transmittance. Meanwhile, the $[BO_3]$ and $[B_3O_6]$ groups have large optical anisotropy, which is conducive to the formation of large birefringence.[17–19] Therefore, the borate system represents an excellent source for the exploration of DUV birefringent crystals.[20–27] It is known that π-conjugated units such as $[BO_3]$,[28] $[B_3O_6]$,[29] $[CO_3]$,[30] $[NO_3]$[31] and $[C_3N_3O_3]$[32] can produce enough optical anisotropy, resulting in large birefringence. However, the so-called dangling bonds of these π-conjugated units reduce the band gap, which limits their DUV transmittance window. To solve the problem,

[a]*College of Chemistry and Materials Science, Hebei Research Center of the Basic Discipline of Synthetic Chemistry, Key Laboratory of Medicinal Chemistry and Molecular Diagnosis of the Ministry of Education, Key Laboratory of Chemical Biology of Hebei Province, Hebei University, Baoding 071002, China.*
E-mail: wangy@hbu.edu.cn
[b]*Institute of Life Science and Green Development, Hebei University, Baoding 071002, China*

†Electronic supplementary information (ESI) available. CCDC 2356772 and 2356774. For ESI and crystallographic data in CIF or other electronic format see DOI: https://doi.org/10.1039/d4qi01530d

the π-conjugated units must connect with other functional groups by covalence bonds in order to remove the dangling bonds. Recently, Chen *et al.* proposed a confined π-conjugated strategy, in which π-conjugated groups should be connected by non-π-conjugated groups to weaken the interaction of π-conjugated groups.[33] In addition, in order to increase birefringence, the π-conjugated units should be arranged in a suitable way in the crystal structure.[34] In addition, it is reported that the introduction of secondary building units such as $[BO_4]$,[22] $[BO_3F]$,[22] $[BeO_4]$,[35] and $[PO_4]$,[36] can help the rational arrangement of the π-conjugated units. However, in previous efforts, it was difficult to increase the band gap and birefringence simultaneously.

In this work, we propose a strategy to enhance the contradictory properties of DUV birefringent materials by combining an extended π-conjugated unit with newly developed [Al–O/F] functional units. It is known that the $[B_3O_6]$ unit has a larger π-conjugated system compared to $[BO_3]$, which is beneficial to produce large birefringence. When a large electronegativity F atom is further introduced, Al atoms can be combined with O/F atoms to form complex and diverse [Al–O/F] functional groups.[37] The [Al–O/F] group has three advantages: (1) replacing O with a more electronegative F can increase the band gap and optical anisotropy compared to aluminoborate; (2) the rich coordination environment in [Al–O/F] groups provides more structural possibilities; and (3) compared with other fluoroborates, fluoroaluminoborates generally have better thermal stability, and it is easier to obtain large crystals in open systems.[38] Thus, fluoroaluminoborates containing both π-conjugated units and [Al–O/F] functional groups could be a new source for DUV birefringent materials.

To verify the above idea, $BaAlBO_3F_2$,[39] a famous nonlinear optical crystal with a small birefringence, was selected as a prototype. Before this work, $BaAlBO_3F_2$ was the only known compound in the Ba–Al–B–O–F system, with a band gap of 7.52 eV and a frequency doubling response of 2 times KDP. However, its birefringence is only 0.042@546 nm, and DUV phase matching cannot be realized. Therefore, this system has potential and requires further exploration. Two new alkali-earth fluoroaluminoborates $BaAlB_3O_6F_2$ and $BaAl_2(B_3O_6)_2F_2$ were discovered through the comprehensive exploration of Ba–Al–B–O–F. From $BaAlBO_3F_2$ to $BaAlB_3O_6F_2$ and $BaAl_2(B_3O_6)_2F_2$, it was demonstrated that a large band gap and birefringence can be simultaneously achieved by the rational combination of extended π-conjugated $[B_3O_6]$ and $[AlO_3F]$ groups. In addition, the single crystal structure and thermal and optical properties of the two materials were characterized and analyzed.

Experimental section

Reagents

BaF_2, Al_2O_3, H_3BO_3 (analytically pure, Aladdin Chemical Industry Co., Ltd) and AlF_3 (99%, Rhawn Chemical Industry Co., Ltd) were used without further processing.

Synthesis

The synthesis of $BaAlB_3O_6F_2$ and $BaAl_2(B_3O_6)_2F_2$ was carried out using the high-temperature solution method, yielding single crystals of the compounds. For $BaAlB_3O_6F_2$, the starting materials were BaF_2 (0.7013 g, 4 mmol), Al_2O_3 (0.2039 g, 4 mmol), and H_3BO_3 (1.1129 g, 18 mmol), which were mixed and ground before being placed in an alumina crucible. The temperature increased to 770 °C over a period of 8 h, was maintained at this temperature for 12 h, and cooled to room temperature at a rate of 105 °C h^{-1}. For $BaAl_2(B_3O_6)_2F_2$, BaF_2 (1.038 g, 6 mmol), AlF_3 (0.497 g, 6 mmol), and H_3BO_3 (1.465 g, 24 mmol) were mixed and ground, heated to 850 °C in 8 h, held for 6 h and cooled to 650 °C at 2 °C per hour before finally being cooled to room temperature. Small, colourless crystals of $BaAlB_3O_6F_2$ and $BaAl_2(B_3O_6)_2F_2$ were obtained from the products for structural determination.

The polycrystalline crystal of $BaAlB_3O_6F_2$ was obtained using the same conditions as used for the single crystal synthesis. The products were further washed with hot water to remove excess boric acid before the test. Polycrystalline samples of $BaAl_2(B_3O_6)_2F_2$ were prepared by the conventional solid-state method using stoichiometric ratios of raw materials. The mixed sample was subjected to a 2 h preheat at 510 °C, followed by 4 h calcination at 830 °C, and finally cooled to room temperature. It is noted that the synthesis of $BaAl_2(B_3O_6)_2F_2$ is sensitive to temperature and holding time. An inappropriate calcination temperature or longer holding time will decrease the purity and crystallinity.

Single-crystal structure determination

Single-crystal data for $BaAlB_3O_6F_2$ and $BaAl_2(B_3O_6)_2F_2$ were collected on a Bruker D8 VENTURE diffractometer equipped with a Mo IμS 3.0 microfocus X-ray source (λ = 0.71073 Å). Integration and absorption correction of the single-crystal data were performed using the SAINT program and processed using Olex2.[40] The structure was solved using the intrinsic phase method and refined using least squares techniques. The structure was checked for possible higher symmetry using PLATON.[41] The crystal data and detailed refinement information are given in Table S1.† The atom positions, isotropic displacement parameters, and bond valence sums of each atom are presented in Tables S2 and S3† for $BaAlB_3O_6F_2$ and $BaAl_2(B_3O_6)_2F_2$, respectively. Selected bond distances and angles are summarized in Tables S4–S7.†

Powder XRD

Powder XRD was performed on a Haoyuan DX-27 mini X-ray diffractometer with Cu Kα radiation (λ = 1.54056 Å) at room temperature. The scanning was done with the 2θ angles in the interval 5–70°, a scan step width of 0.02°, and a fixed counting time of 2 s.

Thermal analysis

The thermal gravimetric (TG) analysis and differential scanning calorimetry (DSC) of $BaAlB_3O_6F_2$ and $BaAl_2(B_3O_6)_2F_2$ were

performed with a HENVEN HCT-2 instrument under flowing air. The sample was placed in an Al_2O_3 crucible and heated from 30 to 1100 °C with a heating rate of 10 °C min^{-1}.

Infrared spectroscopy

The IR spectra of $BaAlB_3O_6F_2$ and $BaAl_2(B_3O_6)_2F_2$ were recorded on a Shimadzu IR Affinity-1 Fourier transform infrared spectrometer in the range of 400–4000 cm^{-1}. The sample was mixed with KBr and ground well.

UV–vis–NIR diffuse reflectance spectrum

The diffuse reflectance spectrum was measured at room temperature with a Shimadzu UV-2600i UV spectrophotometer in the 200–1100 nm wavelength range.

Birefringence measurements

The birefringence was assessed with a polarizing microscope (NIKON Eclipse Ci-POL) equipped with a quartz wedge compensator under a light source of 546 nm. According to the equation, R (retardation) = $\Delta n \times d$, the birefringence was calculated, where R, Δn, and d represent the optical path difference, birefringence, and thickness of the crystal, respectively. The thickness of the crystalline sample was measured on a single-crystal XRD diffractometer.

Theoretical calculations

The electronic structures and optical properties for $BaAlB_3O_6F_2$ and $BaAl_2(B_3O_6)_2F_2$ were calculated using the CASTEP package.[42] The generalized gradient approximation (GGA) with the Perdew–Burke–Ernzerhof (PBE) functional was selected as the exchange–correlation potential.[43] The norm-conserving pseudopotentials (NCP) were adopted.[44] The cutoff energy was set as 850 eV for both compounds. The dense k-points in the Brillouin zone were set as 2 × 1 × 2 and 2 × 2 × 1 for $BaAlB_3O_6F_2$ and $BaAl_2(B_3O_6)_2F_2$, respectively. The configurations for diverse electron orbitals were Ba: $5s^25p^66s^2$, Al: $3s^23p^1$, B: $2s^22p^1$, O: $2s^22p^4$, and F: $2s^22p^5$, respectively. The GGA method usually underestimates the band gaps of crystals; therefore, the HSE06 method was also adopted to evaluate the band gap.[45]

Results and discussion

Crystal structure

$BaAlB_3O_6F_2$ crystallized in monoclinic space group $P2_1/c$ with the cell parameters a = 7.1245(6) Å, b = 12.708(1) Å, c = 7.6246(7) Å, and β = 112.189(3) Å (Table S1†). In this structure, one Ba atom, one Al atom, three B atoms, six O atoms, and two F atoms are combined to form an asymmetric unit. One Ba atom is coordinated with six O atoms and four F atoms to form $[BaO_6F_4]$ polyhedron (Fig. 1a). The B atom is connected with three O atoms to form $[BO_3]$ groups, and these $[BO_3]$ groups are connected to each other to form a one-dimensional $[BO_3]_\infty$ chain structure (Fig. 1d). The independent Al atom forms a *trans*-$[AlO_4F_2]$ octahedron with four O atoms and two F atoms.

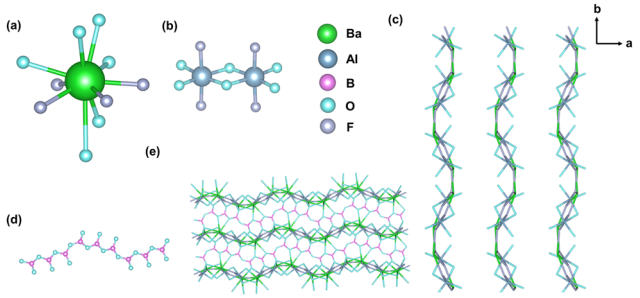

Fig. 1 (a) The coordination environment of the Ba atom. (b) The $[Al_2O_6F_4]$ group formed by the connection of two $[AlO_4F_2]$ octahedra. (c) The layered structure formed by the connection of the $[BaO_6F_4]$ polyhedron and $[AlO_4F_2]$ group in the c direction. (d) $[BO_3]$ are connected to each other to form an infinite chain. (e) The 3D framework structure of $BaAlB_3O_6F_2$.

The F atoms are located at opposite positions of the octahedron with the Al–O bond lengths ranging from 1.8458 to 1.8995 Å and the Al–F bond lengths ranging from 1.8088 to 1.8130 Å. The two *trans*-$[AlO_4F_2]$ octahedra are connected to form the $[Al_2O_6F_4]$ group by sharing two O atoms (Fig. 1b), and the $[BaO_6F_4]$ polyhedra are connected to each other through an O and an F in $[AlO_4F_2]$ to form a layered structure (Fig. 1c). Such cationic layers are connected to each other through a $[BO_3]_\infty$ chain to form a three-dimensional frame (Fig. 1e). The bond valence sum (BVS) was calculated for all atoms of $BaAlB_3O_6F_2$ (Table S2†). The calculated results are consistent with their valences, which also proves the rationality of the structural model.

$BaAl_2(B_3O_6)_2F_2$ crystallized in trigonal space group $R\bar{3}c$ with cell parameters a = 7.0654(18) Å, b = 7.0654(18) Å, c = 37.529(13) Å (Table S1†). In the asymmetric unit, the unique Ba atom coordinates with 12 O atoms and 2 F atoms to form the $[BaO_{12}F_2]$ polyhedron (Fig. 2a). The B atoms combine with three O atoms to form a plane $[BO_3]$ triangle. The Al atoms combine with three O atoms and one F atom to form the distorted $[AlO_3F]$ tetrahedron with an Al–O bond length of 1.743 Å and an Al–F bond length of 1.664 Å. Three $[BO_3]$ and one $[AlO_3F]$ units are connected by shared O atoms to form $[AlB_3O_6F]$ basic building blocks (Fig. 2b), which are connected to each other forming a two-dimensional $[AlB_3O_6F]$ infinite layer. The $[AlB_3O_6F]$ layers are further connected *via* $[BaO_{12}F_2]$ polyhedra to form a 3D framework structure (Fig. 2c), and Ba atoms are filled between the $[AlB_3O_6F]$ layers. The BVS calculation results of $BaAl_2(B_3O_6)_2F_2$ also validate the structural correctness.

The crystal structure of $BaAlB_3O_6F_2$ exhibits a unique structure type similar to that of $SrAlB_3O_6F_2$,[46] while the structure of $BaAl_2(B_3O_6)_2F_2$ is very close to those of $KBe_2BO_3F_2$ and $BaAlBO_3F_2$. Fig. 2d and e show the 3D framework structure of $KBe_2BO_3F_2$ and $BaAlBO_3F_2$ in the a direction, respectively. It can be seen that $BaAl_2(B_3O_6)_2F_2$, $KBe_2BO_3F_2$ and $BaAlBO_3F_2$ show similar layered structural features. In $KBe_2BO_3F_2$,[47] $[BeO_3F]$ and $[BO_3]$ are connected to form a layered structure, and K atoms are filled between the layers. $BaAl_2(B_3O_6)_2F_2$ has changed its original structure by replacing $[BeO_3F]$ with

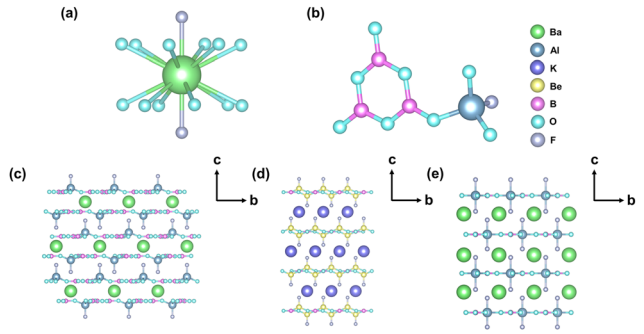

Fig. 2 (a) The coordination environment of the Ba atom. (b) The basic building block of [AlB_3O_6F] formed by the connection of [B_3O_6] and [AlO_3F] groups. Crystal structures of (c) $BaAl_2(B_3O_6)_2F_2$, (d) $KBe_2BO_3F_2$, and (e) $BaAlBO_3F_2$ in the *a* direction.

[AlO_3F] and [BO_3] with [B_3O_6], and K cations are substituted by Ba cations.

In addition, the [Al–O/F] functional units are [AlO_3F_2], [AlO_4F_2], [AlO_3F], in which the central Al atoms adopts sp^3d, sp^3d^2, and sp^3 hybridization, for $BaAlBO_3F_2$, $BaAlB_3O_6F_2$, and $BaAl_2(B_3O_6)_2F_2$, respectively. Fig. S1† shows the different arrangements of [Al–O/F] groups in $BaAlBO_3F_2$, $BaAlB_3O_6F_2$, and $BaAl_2(B_3O_6)_2F_2$. The layered structure in $BaAlBO_3F_2$ is composed of the connection of [AlO_3F_2] to the [BO_3] group. Different from $BaAlBO_3F_2$, the layered structure in $BaAlB_3O_6F_2$ is composed of the connection of the [BO_3] chain to [AlO_4F_2]. The layered structure in $BaAl_2(B_3O_6)_2F_2$ is composed of [AlO_3F] connected to the [B_3O_6] group, which greatly increases its optical anisotropy, resulting in a large birefringence.

PXRD and thermal properties

The synthesis of polycrystalline samples of $BaAlB_3O_6F_2$ is not straightforward, while $BaAl_2(B_3O_6)_2F_2$ can be obtained easily. Initially, according to the stoichiometric ratio of $BaAlB_3O_6F_2$, only the known compound $BaAlBO_3F_2$ can be obtained. Then, on the basis of the stoichiometric ratio, 50% additional boric acid can be added to obtain the pure phase of $BaAlB_3O_6F_2$. However, if the pure phase of $BaAlBO_3F_2$ is synthesized, it is not possible to transform it to $BaAlB_3O_6F_2$ by adding the same amount of boron oxide, even under different calcination conditions. It is speculated that $BaAlBO_3F_2$ is a very stable compound, and no other reaction can occur if it is generated. $BaAlB_3O_6F_2$ can only be formed by the initial addition of excess boron oxide as a flux. Phase analysis of the prepared $BaAlB_3O_6F_2$ and $BaAl_2(B_3O_6)_2F_2$ was carried out. As shown in Fig. S2,† the experimental patterns of $BaAlB_3O_6F_2$ and $BaAl_2(B_3O_6)_2F_2$ are in good agreement with their simulated XRD patterns. The thermal analysis of $BaAlB_3O_6F_2$ and $BaAl_2(B_3O_6)_2F_2$ demonstrated that both of them have high thermal stability, with a maximum weight loss of 3% before 950 °C (Fig. S3†). Their thermogravimetric results revealed endothermic peaks at 880 and 810 °C, respectively. The pure phases of $BaAlB_3O_6F_2$ and $BaAl_2(B_3O_6)_2F_2$ were melted and cooled to room temperature slowly. It was found that they formed an amorphous phase after melting although the thermogravimetric curves showed no weight loss. Because of the high viscosity of boron-rich melt, it is necessary to introduce additional flux to perform crystal growth.

Spectrum analysis

The infrared spectra of $BaAlB_3O_6F_2$ and $BaAl_2(B_3O_6)_2F_2$ are presented in Fig. S4a and S4b,† respectively. For $BaAlB_3O_6F_2$, the strong absorption band between 1470 and 1150 cm^{-1} can be attributed to the asymmetric stretching of the [BO_3] group, while the peaks near 958 and 924 cm^{-1} can be attributed to the symmetric stretching of [BO_3]. The peaks at 756 and 700 cm^{-1} belong to the bending vibration of [BO_3], and the peaks between 600 and 400 cm^{-1} are mainly caused by the stretching bending vibration of [AlO_4F_2]. For $BaAl_2(B_3O_6)_2F_2$, the peaks at 1300 cm^{-1} and 1400 cm^{-1} are due to the asymmetric stretching of the [BO_3] group, while the peaks at 1010 cm^{-1} and 1090 cm^{-1} are mainly related to the symmetric stretching vibration of the [BO_3] group. The peaks at 835 cm^{-1} and 727 cm^{-1} correspond to the out-of-plane bending of the [BO_3] group, and the peaks at 696 cm^{-1} and 469 cm^{-1} may correspond to the stretch-bending vibration of the [AlO_3F] group. The test results clearly demonstrate that $BaAlB_3O_6F_2$ and $BaAl_2(B_3O_6)_2F_2$ have completely different fundamental building units, which is consistent with the single crystal XRD structure analysis.

The UV–vis–NIR spectra of $BaAlB_3O_6F_2$ and $BaAl_2(B_3O_6)_2F_2$ demonstrate that both of them do not exhibit any absorption peak before 200 nm. This observation indicates that the UV cut off edge of $BaAlB_3O_6F_2$ and $BaAl_2(B_3O_6)_2F_2$ is less than 200 nm (Fig. 3). The reasons for the large band gap of $BaAlB_3O_6F_2$ and $BaAl_2(B_3O_6)_2F_2$ can be attributed to the following factors: (1) the valence electrons of Ba^{2+} do not contain d–d and f–f transitions; (2) the introduction of fluorine widens the band gap; and (3) the absence of dangling bonds in the [BO_3] and [B_3O_6] groups further increases the band gap.

Birefringence measurements

Due to the [BO_3] ring structure of $BaAlB_3O_6F_2$ and the [B_3O_6] ring structure of $BaAl_2(B_3O_6)_2F_2$, both materials are predicted to have large birefringence. The birefringence of $BaAlB_3O_6F_2$ and $BaAl_2(B_3O_6)_2F_2$ was measured using a Nikon polarizing

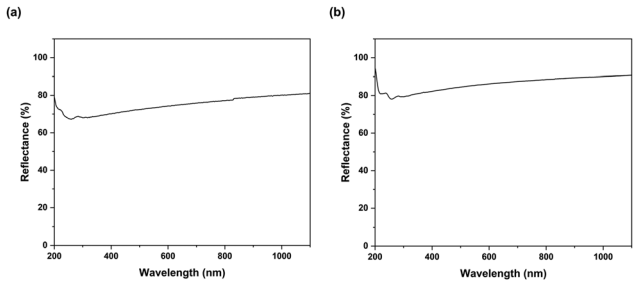

Fig. 3 UV–vis–NIR diffuse reflectance spectra of (a) $BaAlB_3O_6F_2$ and (b) $BaAl_2(B_3O_6)_2F_2$.

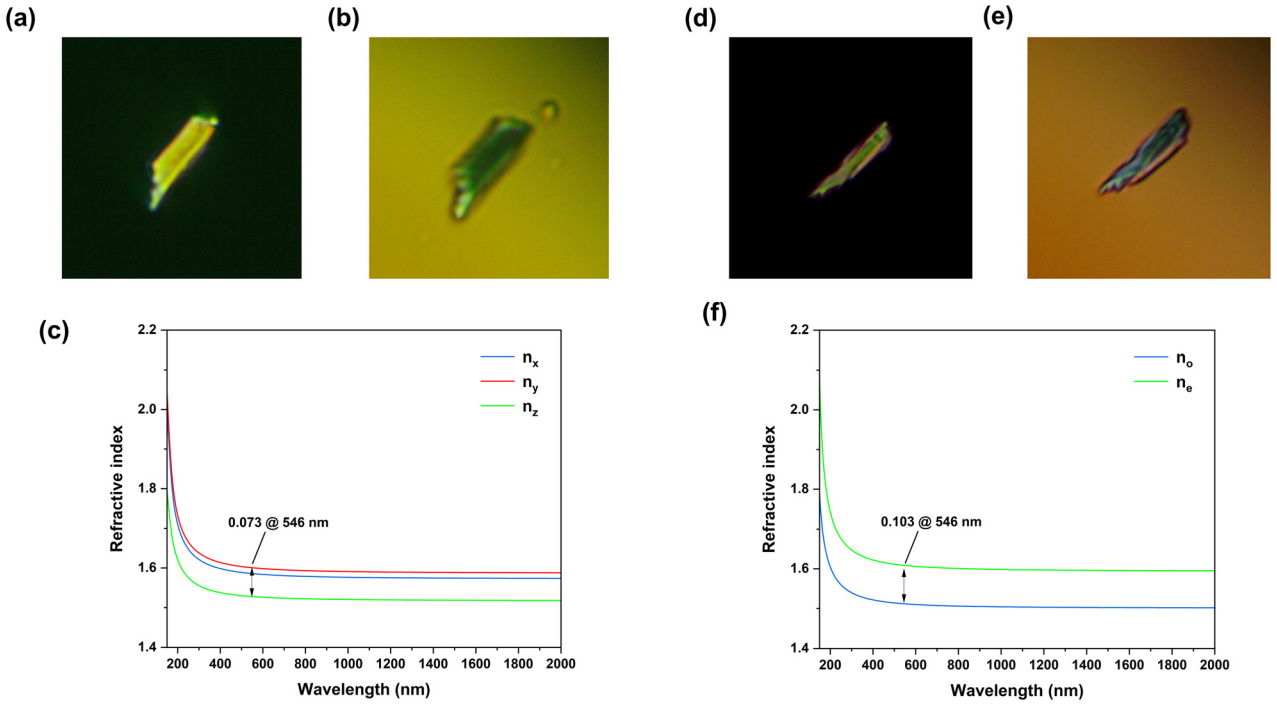

Fig. 4 Photos of the original (a) $BaAlB_3O_6F_2$ crystal and (d) $BaAl_2(B_3O_6)_2F_2$ crystal. Photos of (b) the $BaAlB_3O_6F_2$ crystal and (e) the $BaAl_2(B_3O_6)_2F_2$ crystal after extinction. The calculated refractive indices of (c) $BaAlB_3O_6F_2$ and (f) $BaAl_2(B_3O_6)_2F_2$.

microscope under cross-polarized light. Their crystal picture and the image after extinction are shown in Fig. 4. The experimental results show that the crystal interference color of $BaAlB_3O_6F_2$ observed under polarized light is fifth-order yellow. According to the Michel–Levy interference color diagram, its optical path difference is 2.53 μm and the crystal thickness (d) is 29 μm (Fig. S5a†). Therefore, according to the relationship $\Delta n = R/d$, the measured birefringence is 0.087 at 546 nm. The interference color of $BaAl_2(B_3O_6)_2F_2$ measured by the same steps is sixth grade yellow, its optical path difference is 3.01 μm and the crystal thickness is 29 μm (Fig. S5b†). Therefore, it has a birefringence of 0.105. Compared with $BaAlBO_3F_2$, the birefringence of the two materials is significantly improved. In order to predict their optical anisotropy, we also use the DFT method to calculate their birefringence. The birefringence values of $BaAlB_3O_6F_2$ and $BaAl_2(B_3O_6)_2F_2$ at 546 nm are 0.073 and 0.097, respectively, which are in good agreement with the measured birefringence. The birefringent properties of $BaAlB_3O_6F_2$ and $BaAl_2(B_3O_6)_2F_2$ are comparable to those of some recently published UV birefringent materials, such as $Ba_{3.75}MgB_7O_{14}F_{2.5}$ (Δn = 0.081@546 nm),[48] $RbSb_2(C_2O_4)F_5$ (Δn = 0.09@546 nm),[49] $Rb[B_3O_3F_2(OH)_2]$ (Δn = 0.09@546 nm),[50] $Ba_2K_{1.6}Na_{0.4}Sc_2(BO_3)_4$ (Δn = 0.11@550 nm),[51] $(NH_4)[C(NH_2)_3][B_3O_3F_4(OH)]$ (Δn = 0.101@1064 nm)[52] and $RbBaScB_6O_{12}$ (Δn = 0.139@550 nm).[53]

$BaAlB_3O_6F_2$ possesses a $[BO_3]_\infty$ chain structure, which has a denser $[BO_3]$ arrangement in comparison with $BaAlBO_3F_2$. By calculating the density per unit volume of $[BO_3]$ in $BaAlBO_3F_2$(0.0155), $BaAlB_3O_6F_2$(0.0188) and $BaAl_2(B_3O_6)_2F_2$(0.027), it is obvious that a higher $[BO_3]$ density is beneficial to increase optical anisotropy, *i.e.*, birefringence. In addition to the density of the $[BO_3]$ groups, the arrangement of the $[BO_3]$ groups also has an effect on the birefringence. Therefore, the dihedral angles between adjacent $[BO_3]$ groups in $BaAlB_3O_6F_2$ and $BaAl_2(B_3O_6)_2F_2$ were calculated. The dihedral angles between adjacent $[BO_3]$ groups in $BaAlB_3O_6F_2$ are 12.454°, 18.069°, and 38.536°, respectively, demonstrating that the $[BO_3]$ groups are not perfectly aligned, while the dihedral angle is almost zero in $BaAl_2(B_3O_6)_2F_2$. Compared to $BaAlBO_3F_2$, $BaAl_2(B_3O_6)_2F_2$ has an extended π-conjugated $[B_3O_6]$ ring, and it contains $[AlO_3F]$ (point group, C_{3v}) units in contrast to highly symmetrical $[AlO_3F_2]$ (point group, D_{3h}) units in $BaAlBO_3F_2$. For $BaAl_2(B_3O_6)_2F_2$, the introduction of the $[B_3O_6]$ ring and its layered structure further increases the birefringence property, while covalently bonded $[AlO_3F]$ units help remove the dangling bonds of [B–O] groups, which inherit the advantages of the large band gap feature of $KBe_2BO_3F_2$ and $BaAlBO_3F_2$.

Theoretical calculations

In order to clarify the relationship between the optical properties and electronic structures, the band structure, density of state and partial density of state (PDOS) of $BaAlB_3O_6F_2$ were calculated using first principles. Considering that GGA underestimates the bandgap of the compound in standard DFT calculations due to the discontinuity of the exchange associated energy, we further corrected the band gaps using the HSE06 method. The results indicate that $BaAlB_3O_6F_2$ and $BaAl_2(B_3O_6)_2F_2$ have wide band gaps of 7.53 and 7.87 eV

(Fig. S6†), respectively, and both of them show an indirect band gap feature. The corresponding UV cutoff edges are 165 and 157.5 nm for $BaAlB_3O_6F_2$ and $BaAl_2(B_3O_6)_2F_2$, respectively. The calculated results are in good agreement with the experimental ones (UV cut off edges < 200 nm). Table S8† shows the bandgap, birefringence and [Al–O/F] arrangement of the currently reported F-containing aluminoborates. Fig. 5 presents a plot of band gap and birefringence values of some F-containing aluminoborates. Notably, $BaAl_2(B_3O_6)_2F_2$ has the largest band gap (7.87 eV) and a large birefringence (Δn = 0.105 at 546 nm) among all known F-containing aluminoborates (including aluminoborate fluorides and fluoroaluminoborates). This demonstrates that $BaAlB_3O_6F_2$ and $BaAl_2(B_3O_6)_2F_2$ are potential DUV birefringent materials.

The PDOS diagram of $BaAlB_3O_6F_2$ is similar to that of $BaAl_2(B_3O_6)_2F_2$ (Fig. 6). For both compounds, the top of the valence bands is mainly composed of O 2p and F 2p orbitals. The bottom of the conduction bands is mainly composed of Ba 5d, Al 3s3p, and B 2s2p orbitals. The difference is that the contribution of the B 2s2p orbitals in $BaAl_2(B_3O_6)_2F_2$ to the valence bands is greater than that in $BaAlB_3O_6F_2$. The high densities and overlaps of Al 3s3p, B 2s2p, O 2p, and F 2p near Fermi level orbitals indicate that the [B–O] and [Al–O/F] groups mainly determine the optical properties of $BaAlB_3O_6F_2$ and $BaAl_2(B_3O_6)_2F_2$.

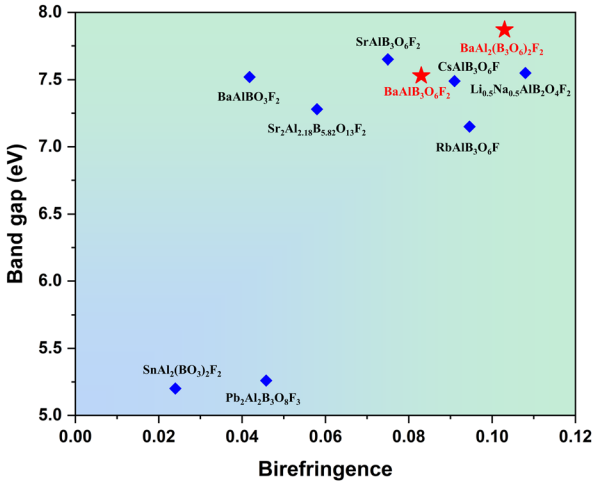

Fig. 5 Comparison of the bandgap and birefringence of F-containing aluminoborates.

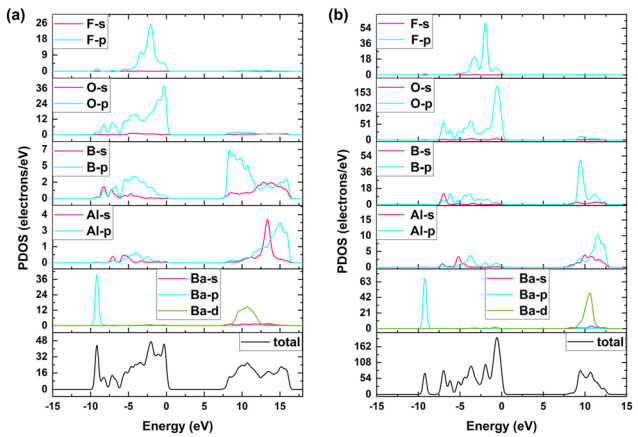

Fig. 6 Calculated total and partial densities of states of (a) $BaAlB_3O_6F_2$ and (b) $BaAl_2(B_3O_6)_2F_2$.

Conclusions

In summary, our work provides two new barium fluoroaluminoborates, $BaAlB_3O_6F_2$ and $BaAl_2(B_3O_6)_2F_2$, as potential DUV birefringent materials. The two crystals were synthesized in an open system through reasonable structural design. It presents a systematic work on the Ba–Al–B–O–F system many years after the discovery of $BaAlBO_3F_2$, which also enriches the fluoroaluminoborate family. Compared with the compound $BaAlBO_3F_2$, the birefringence of the two materials is significantly improved; the birefringence values of $BaAlB_3O_6F_2$ (Δn = 0.087@546 nm) and $BaAl_2(B_3O_6)_2F_2$ (Δn = 0.105@546 nm) are 2 and 2.5 times that of $BaAlBO_3F_2$, respectively. In particular, $BaAl_2(B_3O_6)_2F_2$ have $[AlO_3F]$ and $[B_3O_6]$ rings, which further improve the birefringenc performance on the basis of inheriting the advantages of the large band gap and large birefringence of $KBe_2BO_3F_2$. In addition, among all known F-containing aluminum borates, $BaAl_2(B_3O_6)_2F_2$ exhibits the largest band gap (7.87 eV) among all known F-containing aluminoborates. The first principles calculations demonstrate that the $[AlO_3F]$ tetrahedron and the $[B_3O_6]$ ring make a major contribution to the optical properties of $BaAl_2(B_3O_6)_2F_2$. We reveal that extending π-conjugated units combined with [Al–O/F] functional units can help in the design of DUV birefringent materials. This finding also provides new possibilities for searching DUV birefringent materials in fluoroaluminoborates.

Author contributions

The manuscript was written through the contributions of all authors: conceptualization, Y.W.; methodology, C.C.; software, C.C. and B.Z.; validation, Y.W.; formal analysis, C.C. and Y.B.; investigation, C.C, Y.W.; data curation, C.C and D.D.; writing (original draft preparation), C.C.; writing (review and editing), Y.W.; visualization, C.C.; supervision, Y.W.; project administration, Y.W.; funding acquisition, Y.W., B.Z. All authors have given approval to the final version of the manuscript.

Data availability

- The data supporting this article have been included as part of the ESI.†
- Crystallographic data for $BaAlB_3O_6F_2$ and $BaAl_2(B_3O_6)_2F_2$ has been deposited at the CCDC under 2356772 and 2356774† and can be obtained from **https://www.ccdc.cam.ac.uk/**.

Conflicts of interest

The authors declare no competing financial interest.

Acknowledgements

This work was supported by the National Natural Science Foundation of China (Grant No. 21975062 and 52072109), the Natural Science Foundation of Hebei Province (E2023201017 and B2023201108), and the Excellent Youth Research Innovation Team of Hebei University (QNTD202403).

References

1 M. Mutailipu, K. R. Poeppelmeier and S. L. Pan, Borates: A rich source for optical materials, *Chem. Rev.*, 2020, **121**, 1130–1202.
2 J. D. Yan, D. D. Chu, F. F. Zhang, Z. H. Yang, S. L. Pan and X. L. Hou, Enhancing birefringence of non-π-conjugated sulfate systems through rare-earth metal-centered polyhedra, *CrystEngComm*, 2023, **25**, 2939–2945.
3 K. M. Ok, Toward the rational design of novel noncentrosymmetric materials: factors influencing the framework structures, *Acc. Chem. Res.*, 2016, **49**, 2774–2785.
4 J. Y. Guo, J. B. Huang, A. Tudi, X. L. Hou, S. J. Han, Z. H. Yang and S. L. Pan, Birefringence regulation by clarifying the relationship between stereochemically active lone pairs and optical anisotropy in tin-based ternary halides, *Angew. Chem., Int. Ed.*, 2023, **62**, e202304238.
5 J. Hecht, A short history of laser development, *Opt. Eng.*, 2010, **49**, 091002.
6 A. Tudi, S. J. Han, Z. H. Yang and S. L. Pan, Potential optical functional crystals with large birefringence: Recent advances and future prospects, *Coord. Chem. Rev.*, 2022, **459**, 214380.
7 F. Sedlmeir, R. Zeltner, G. Leuchs and H. G. L. Schwefel, High-Q MgF_2 whispering gallery mode resonators for refractometric sensing in aqueous environment, *Opt. Express*, 2014, **22**, 30934–30942.
8 G. Ghosh, Dispersion-equation coefficients for the refractive index and birefringence of calcite and quartz crystals, *Opt. Commun.*, 1999, **163**, 95–102.
9 G. Q. Zhou, J. Xu, X. D. Chen, H. Y. Zhong, S. T. Wang and K. Xu, Growth and spectrum of a novel birefringent α-BaB_2O_4 crystal, *J. Cryst. Growth*, 1998, **191**, 517–519.
10 H. T. Luo, T. Tkaczyk, E. L. Dereniak, K. Oka and R. Sampson, High birefringence of the yttrium vanadate crystal in the middle wavelength infrared, *Opt. Lett.*, 2006, **31**, 616–618.
11 D. E. Zelmon, D. L. Small and D. Jundt, Infrared corrected sellmeier coefficients for congruently grown lithium niobate and 5 mol% magnesium oxide-doped lithium niobate, *J. Opt. Soc. Am. B*, 1997, **14**, 3319–3322.
12 X. Wang, M. J. Xia and R. K. Li, A promising birefringent crystal $Ba_2Na_3(B_3O_6)_2F$, *Opt. Mater.*, 2014, **38**, 6–9.
13 V. V. Atuchin, S. V. Adichtchev, B. G. Bazarov, Zh G. Bazarova, T. A. Gavrilova, V. G. Grossman, V. G. Kesler, G. S. Meng, Z. S. Lin and N. V. Surovtsev, Electronic structure and vibrational properties of $KRbAl_2B_2O_7$, *Mater. Res. Bull.*, 2013, **48**, 929–934.
14 V. V. Atuchin, L. I. Isaenko, V. G. Kesler, Z. S. Lin, M. S. Molokeev, A. P. Yelisseyev and S. A. Zhurkov, Exploration on anion ordering, optical properties and electronic structure in $K_3WO_3F_3$ elpasolite, *J. Solid State Chem.*, 2012, **187**, 159–164.
15 P. S. Halasyamani and K. R. Poeppelmeier, Noncentrosymmetric oxides, *Chem. Mater.*, 1998, **10**, 2753–2769.
16 H. W. Yu, J. S. Young, H. P. Wu, W. G. Zhang, J. M. Rondinelli and P. S. Halasyamani, Electronic, crystal chemistry, and nonlinear optical property relationships in the dugganite $A_3B_3CD_2O_{14}$ family, *J. Am. Chem. Soc.*, 2016, **138**, 4984–4989.
17 M. Mutailipu and S. L. Pan, Emergent deep-ultraviolet nonlinear optical candidates, *Angew. Chem., Int. Ed.*, 2020, **59**, 20302–20317.
18 Y. Wang and S. L. Pan, Recent development of metal borate halides: Crystal chemistry and application in second-order NLO materials, *Coord. Chem. Rev.*, 2016, **323**, 15–35.
19 Y. Yang, X. X. Jiang, Z. S. Lin and Y. C. Wu, Borate-based ultraviolet and deep-ultraviolet nonlinear optical crystals, *Crystals*, 2017, **7**, 95.
20 Z. Z. Zhang, Y. Wang, B. B. Zhang, Z. H. Yang and S. L. Pan, $CaB_5O_7F_3$: A beryllium-free alkaline-earth fluorooxoborate exhibiting excellent nonlinear optical performances, *Inorg. Chem.*, 2018, **57**, 4820–4823.
21 M. Mutailipu, M. Zhang, B. B. Zhang, L. Y. Wang, Z. H. Yang, X. Zhou and S. L. Pan, $SrB_5O_7F_3$ functionalized with $[B_5O_9F_3]^{6-}$ chromophores: Accelerating the rational design of deep–ultraviolet nonlinear optical materials, *Angew. Chem., Int. Ed.*, 2018, **57**, 6095–6099.
22 X. F. Wang, Y. Wang, B. B. Zhang, F. F. Zhang, Z. H. Yang and S. L. Pan, CsB_4O_6F: A congruent-melting deep-ultraviolet nonlinear optical material by combining superior functional units, *Angew. Chem., Int. Ed.*, 2017, **56**, 14119–14123.
23 G. Q. Shi, Y. Wang, F. F. Zhang, B. B. Zhang, Z. H. Yang, X. L. Hou, S. L. Pan and K. R. Poeppelmeier, Finding the next deep-ultraviolet nonlinear optical material: $NH_4B_4O_6F$, *J. Am. Chem. Soc.*, 2017, **139**, 10645–10648.
24 Y. C. Yue, Y. Y. Zhu, Y. Zhao, H. Tu and Z. G. Hu, Growth and nonlinear optical properties of $GdAl_3(BO_3)_4$ in a flux without molybdate, *Cryst. Growth Des.*, 2015, **16**, 347–350.
25 H. Zhang, M. Zhang, S. L. Pan, Z. H. Yang, Z. Wang, Q. Bian, X. L. Hou, H. W. Yu, F. F. Zhang, K. Wu, F. Yang, Q. J. Peng, Z. Y. Xu, K. B. Chang and K. R. Poeppelmeier, $Na_3Ba_2(B_3O_6)_2F$: next generation of deep-ultraviolet birefringent materials, *Cryst. Growth Des.*, 2014, **15**, 523–529.

26 Z. Jia, N. N. Zhang, Y. Y. Ma, L. W. Zhao, M. J. Xia and R. K. Li, Top-seeded solution growth and optical properties of deep-UV birefringent crystal $Ba_2Ca(B_3O_6)_2$, *Cryst. Growth Des.*, 2017, **17**, 558–562.
27 X. L. Chen, F. F. Zhang, Y. J. Shi, Y. Z. Sun, Z. H. Yang and S. L. Pan, $MBaYB_6O_{12}$(M = Rb, Cs): Two new rare-earth borates with large birefringence and short ultraviolet cutoff edges, *Dalton Trans.*, 2018, **47**, 750–757.
28 S. G. Zhao, P. F. Gong, L. Bai, X. Xu, S. Q. Zhang, Z. H. Sun, Z. S. Lin, M. C. Hong, C. T. Chen and J. H. Luo, Beryllium-free $Li_4Sr(BO_3)_2$ for deep-ultraviolet nonlinear optical applications, *Nat. Commun.*, 2014, **5**, 4019.
29 H. K. Liu, Y. Wang, B. B. Zhang, Z. H. Yang and S. L. Pan, $CsAlB_3O_6F$: A beryllium-free deep-ultraviolet nonlinear optical material with enhanced thermal stability, *Chem. Sci.*, 2020, **11**, 694–698.
30 G. H. Zou, Z. E. Lin, H. M. Zeng, H. Jo, S. Lim, T. You and K. M. Ok, $Cs_3VO(O_2)_2CO_3$: An exceptionally thermostable carbonatoperoxovanadate with an extremely large second-harmonic generation response, *Chem. Sci.*, 2018, **9**, 8957–8961.
31 X. H. Dong, L. Huang, Q. Y. Liu, H. M. Zeng, Z. E. Lin, D. G. Xu and G. H. Zou, Perfect balance harmony in $Ba_2NO_3(OH)_3$: A beryllium-free nitrate as a UV nonlinear optical material, *Chem. Commun.*, 2018, **54**, 5792–5795.
32 X. Hao, C. S. Lin, M. Luo, Y. Q. Zhou, N. Ye and E. Shangguan, $Cs_2Mg(H_2C_3N_3S_3)_4{\cdot}8H_2O$: An excellent birefringent material with giant optical anisotropy in π-Conjugated trithiocyanurate, *Inorg. Chem.*, 2023, **62**, 7611–7616.
33 L. Xiong, L. M. Wu and L. Chen, A general principle for DUV NLO materials: π-conjugated confinement enlarges band gap, *Angew. Chem., Int. Ed.*, 2021, **60**, 25063–25067.
34 H. K. Liu, B. B. Zhang and Y. Wang, Second-order nonlinear optical materials with a benzene-like conjugated π system, *Chem. Commun.*, 2020, **56**, 13689–13701.
35 S. C. Wang, N. Ye, W. Li and D. Zhao, Alkaline beryllium borate $NaBeB_3O_6$ and $ABe_2B_3O_7$ (A = K, Rb) as UV nonlinear optical crystals, *J. Am. Chem. Soc.*, 2010, **132**, 8779–8786.
36 J. Lu, J. N. Yue, L. Xiong, W. K. Zhang, L. Chen and L. M. Wu, Uniform alignment of non-π-conjugated species enhances deep ultraviolet optical nonlinearity, *J. Am. Chem. Soc.*, 2019, **141**, 8093–8097.
37 J. H. Jiao, M. Zhang and S. L. Pan, Aluminoborates as nonlinear optical materials, *Angew. Chem., Int. Ed.*, 2023, **62**, e202217037.
38 Q. F. Li, W. F. Chen, Y. Z. Lan and J. W. Cheng, Recent progress in ultraviolet and deep-ultraviolet nonlinear optical aluminoborates, *Chin. J. Struct. Chem.*, 2023, **42**, 100036.
39 Z. G. Hu, M. Yoshimura, K. Muramatsu, Y. Mori and T. Sasaki, A new nonlinear optical crystal-$BaAlBO_3F_2$(BABF), *Jpn. J. Appl. Phys.*, 2002, **41**, L1131–L1133.
40 O. V. Dolomanov, L. J. Bourhis, R. J. Gildea, J. A. K. Howard and H. Puschmann, OLEX2: A complete structure solution, refinement and analysis program, *J. Appl. Crystallogr.*, 2009, **42**, 339–341.
41 A. L. Spek, Single-crystal structure validation with the program PLATON, *J. Appl. Crystallogr.*, 2003, **36**, 7–13.
42 J. C. Stewart, D. S. Matthew, J. P. Chris, J. H. Phil, I. J. P. Matt, R. Keith and C. P. Mike, First principles methods using CASTEP, *Z. Kristallogr.*, 2005, **220**, 567–570.
43 J. S. Lin, A. Qteish, M. C. Payne and V. Heine, Optimized and transferable nonlocal separable ab initio pseudopotentials, *Phys. Rev. B: Condens. Matter Mater. Phys.*, 1993, **47**, 4174–4180.
44 A. M. Rappe, K. M. Rabe, E. Kaxiras and J. D. Joannopoulos, Optimized pseudopotentials, *Phys. Rev. B: Condens. Matter Mater. Phys.*, 1990, **41**, 1227–1230.
45 Z. S. Lin, X. X. Jiang, L. Kang, P. F. Gong, S. Y. Luo and M.-H. Lee, First-principles materials applications and design of nonlinear optical crystals, *J. Phys. D: Appl. Phys.*, 2014, **47**, 253001.
46 S. Bai, X. D. Zhang, B. B. Zhang, L. Li and Y. Wang, $SrAlB_3O_6F_2$: A fluoroaluminoborate with $[Al_2B_6O_{14}F_4]$ units and large birefringence, *Inorg. Chem.*, 2021, **60**, 10006–10011.
47 J. Y. Wang, C. Q. Zhang, Y. G. Liu, J. X. Zhang, X. B. Hu, M. H. Jiang, C. T. Chen, Y. C. Wu and Z. Y. Xu, Growth and properties of $KBe_2BO_3F_2$ crystal, *J. Mater. Res.*, 2003, **18**, 2478–2485.
48 Y. J. Bai, X. Y. Wang, H. B. Huang, D. Y. Dou, C. Chen, B. B. Zhang and Y. Wang, $Ba_{3.75}MgB_7O_{14}F_{2.5}$: A mixed alkaline-earth metal borate fluoride with short ultraviolet cutoff edge and large birefringence, *Inorg. Chem.*, 2023, **62**, 15293–15299.
49 W. Y. Wang, X. Y. Wang, L. Xu, D. Zhang, J. L. Xue, S. Y. Wang, X. H. Dong, L. L. Cao, L. Huang and G. H. Zou, Centrosymmetric $Rb_2Sb(C_2O_4)_{2.5}(H_2O)_3$ and noncentrosymmetric $RbSb_2(C_2O_4)F_5$: Two antimony(III) oxalates as UV optical materials, *Inorg. Chem.*, 2023, **62**, 13148–13155.
50 Z. Q. Chen, F. M. Li, Y. L. Liu, C. Cui and M. Mutailipu, Heterologous isomorphic substitution induces optical property enhancement for deep-UV crystals: a case in Rb $[B_3O_3F_2(OH)_2]$, *Inorg. Chem.*, 2023, **62**, 14512–14517.
51 J. F. Zhou, P. F. Gong, M. J. Xia, A. M. Ji, L. F. Zhang, H. Q. Wu and Q. Wu, Atomic substitution to tune ScO_6 distortion in $Ba_2MSc_2(BO_3)_4$ (M = Na, K, Ba) to acquire a large birefringence, *Inorg. Chem.*, 2023, **62**, 8931–8939.
52 Z. Q. Chen, F. M. Li, Z. H. Yang, S. L. Pan and M. Mutailipu, Hydroxyfluorooxoborate $(NH_4)[C(NH_2)_3][B_3O_3F_4(OH)]$ for exploring the effects of cation substitution on structure and optical properties, *Chem. Commun.*, 2023, **59**, 12435–12438.
53 W. H. Liu, P. F. Gong, W. Q. Huang, M. R. Sun, S. G. Zhao, Z. S. Lin and J. Y. Yao, Mixed alkali metal and alkaline earth metal scandium borate birefringence material with layered structure and short ultraviolet cutoff edge, *Inorg. Chem.*, 2023, **62**, 10461–10469.